1 Introduction

Andrew S. Goudie

As Rosenfeld (2004, p. 423) wrote, 'A significant practical contribution of geomorphology is the identification of stable landforms and sites with a low probability of catastrophic or progressive involvement with natural or man-induced processes adverse to human occupance or use. Hazards exist when landscape developing processes conflict with human activity, often with catastrophic results.' Geomorphic events can kill people and damage property. Although high-magnitude, low-frequency catastrophic events, such as hurricanes or earthquakes, gain attention because of the immediacy of large numbers of casualties and great financial losses, there are many more pervasive geomorphological changes that are also of great significance for human welfare. These may have a slower speed of onset, a longer duration, a wider spatial extent and a greater frequency of occurrence. Examples include weathering phenomena and soil erosion. In this volume we discuss both types of geomorphological hazard: the catastrophic and the pervasive.

Indeed, there is a great diversity of geomorphological hazards. One major category is mass movements, such as rockfalls, debris flows, landslides and avalanches. There are also various fluvial hazards, such as floods and river channel changes (e.g. avulsion). In volcanic areas there are disasters caused by eruptions, lava flows, ash falls and lahars. Seismic activity is another type of hazard associated with tectonic activity. In coastal environments one has inundation and erosion caused by storm surges, rapid coastal erosion and siltation, sand and dune encroachment, shoreline retreat and sea-level rise. In glacial areas hazards may be posed by such phenomena as glacial surges, outwash floods and damming of drainage. Permafrost regions may be hazardous because of ground heave, thermokarst development, icings and other such phenomena. There is also a wide range of subsidence hazards caused by solution of limestone, dolomites and evaporites (e.g. gypsum or halite), degradation of organic soils, hydrocompaction of sediments and anthropogenic removal of groundwater and hydrocarbons. In desert regions hazards are posed by wind erosion and deflation of susceptible surfaces, dust storm generation, and by dune migration. More generally, water erosion causes soil loss and gully or badland formation, while weathering can be a threat to a wide range of engineering structures.

The incidence of such hazards can be increased or triggered by human activities, and in particular by land use and land cover changes. There is also an increasing concern that the incidence of hazards will be changed in a warmer world. However, another important consideration is the extent to which human societies are placing themselves at an increased risk as population levels increase and new areas are exploited or settled. Potentially hazardous areas, such as floodplains or steep, deeply weathered slopes, may become occupied, placing human groups at risk. Large urban populations may be especially at risk (see, for example Cooke, 1984). There is evidence that for these sorts of reasons, damage to property and loss of life caused by geomorphological hazards are increasing (Alcántara-Ayala, 2002).

The roles of the geomorphologist in hazard research are many. Of great importance are: the mapping of hazard-prone areas (Griffiths, 2001); constructing the history of occurrence of past hazardous events; establishing their frequency and magnitude; predicting the occurrence and location of future events; monitoring geomorphological change; and using knowledge of the dynamics of geomorphological processes to advise on appropriate mitigation strategies.

In recent years the capabilities of geomorphologists in these roles have increased and the application of

Geomorphological Hazards and Disaster Prevention, eds. Irasema Alcántara-Ayala and Andrew S. Goudie. Published by Cambridge University Press.

geomorphology to the solution of environmental problems has developed (e.g. Cooke and Doornkamp, 1990). Techniques such as remote sensing and Geographic Information Systems (GIS), dating by means, for example, of lichenometry, luminescence dating and dendrochronology, instrumentation of slopes and other phenomena with data-loggers, and computer modelling have all made major contributions. Particularly since the 1960s geomorphologists have become far more knowledgeable about processes and the mechanisms of geomorphological change. They have also become more aware, by adopting a systems framework, of the inter-relationships between different phenomena and of feedback loops, some positive. Concepts of resilience and sensitivity have also been explored (Brunsden, 2001). In addition, a greater awareness has developed of the temporal variability of climate and the implications that this has for understanding geomorphological change (Viles and Goudie, 2003). Related to this has been a burgeoning interest in the way in which human actions can transform geomorphological systems (Goudie, 2006). These are all themes that emerge in the individual chapters of this volume.

References

Alcántara-Ayala, I. (2002). Geomorphology, natural hazards, vulnerability and prevention of natural disasters in developing countries. *Geomorphology*, **47**, 107–124.

Brunsden, D. (2001). A critical assessment of the sensitivity concept in geomorphology. *Catena*, **42**, 99–123.

Cooke, R. U. (1984). *Geomorphological Hazards in Los Angeles*. London: Allen and Unwin.

Cooke, R. U. and Doornkamp, J. C. (1990). *Geomorphology in Environmental Management*, 2nd edition. Oxford: Oxford University Press.

Goudie, A. S. (2006). *The Human Impact on the Natural Environment*, 6th edition. Oxford: Blackwell Publishing.

Griffiths, J. S. (ed.) (2001). *Land Surface Evaluation for Engineering Practice*. Geological Society Engineering Geology Special Publication, 18.

Rosenfeld, C. L. (2004). Geomorphological hazard. In A. S. Goudie (ed.), *Encyclopedia of Geomorphology*. London and New York: Routledge, pp. 423–427.

Viles, H. A. and Goudie, A. S. (2003). Interannual, decadal, and multidecadal scale climatic variability and geomorphology. *Earth-Science Reviews*, **61**, 105–131.

Part I
Processes

2 Regional seismic shaking hazards in mountains

William B. Bull

2.1 Introduction

The steep, crumbly and wet mountains of New Zealand have frequent mass movements and floods, and landscape instability related to glaciers. The Southern Alps sit astride the Australian–Pacific plate boundary (Figure 2.1) with its highly active dextral-oblique thrust faults, active volcanoes, and subduction zones. This chapter summarizes a hazardous geomorphological consequence of widespread seismic shaking in the South Island of New Zealand.

Rocks tumble downhill during earthquakes and the times of arrival on a scree slope can be dated by measuring the largest lichen of *Rhizocarpon* subgenus *Rhizocarpon* on many blocks. This discussion focuses on how to use lichenometry to better understand the intensity and history of hazardous seismic shaking so as to minimize risk. A typical study site is described, the precision of dating is noted, and maps revealing areal intensities of seismic shaking are examined to better understand sizes and sequences of earthquakes.

2.2 Lichenometry site characteristics

The Mt. John site summarizes the desirable features needed for seismic-hazard evaluations. The valley side here was trimmed by a late Pleistocene glacier, creating cliffy outcrops of crumbly greywacke sandstone that have shed blocks to be stored in talus accumulation areas. Hazards such as snow avalanches and water floods are absent. I would have chosen an active talus cone if I had wanted to study the frequency and sizes of avalanches. *Rhizocarpon* subgenus *Rhizocarpon* grows well at this altitude and climate, but locally is impinged upon by other lichens and by mosses.

Each tongue of scree between the bands of dark bushes (Figure 2.2) was inspected for blocks with isolated, circular to elliptical lichens (Figure 2.3) with longest axes clearly demarcated with abrupt margins suitable for measurement with digital calipers. Only the largest *Rhizocarpon* subgenus *Rhizocarpon* was measured on each of the blocks, which range in size from 0.2 to 2 m. The number of lichens to evaluate and choose from generally increased with block size.

As a quality control measure, I made a subjective evaluation of the relative quality of each lichen-size measurement. The main questions to be answered were:

1. Is this really a single thallus, or have several lichens grown together?
2. Is the lichen sufficiently well preserved to reveal the endpoints of the longest axis of growth?
3. Are the margins at the two measurement points sharp and well defined?

Assigned quality control numbers range from 1 to 4:

1. A superb lichen – nearly circular single thallus with abrupt prothallus rims at the two measuring points – that has you reaching for your camera to take a picture of it.
2. Close to ideal for a reliable lichen-size measurement.
3. Nothing special but we feel quite comfortable in including it in the dataset.
4. We hesitate about including this lichen size in the dataset; it has borderline characteristics.

The lichens shown in Figure 2.3 are only of quality class 3, but the rating was raised to 2 because of the presence of a second lichen on this block of about the same size as the largest lichen.

A dataset of 546 lichen-size measurements was collected in 2008. The longest axes range from 6 to 137 mm (age range is AD 1150 to 1980). I have been

Geomorphological Hazards and Disaster Prevention, eds. Irasema Alcántara-Ayala and Andrew S. Goudie. Published by Cambridge University Press.

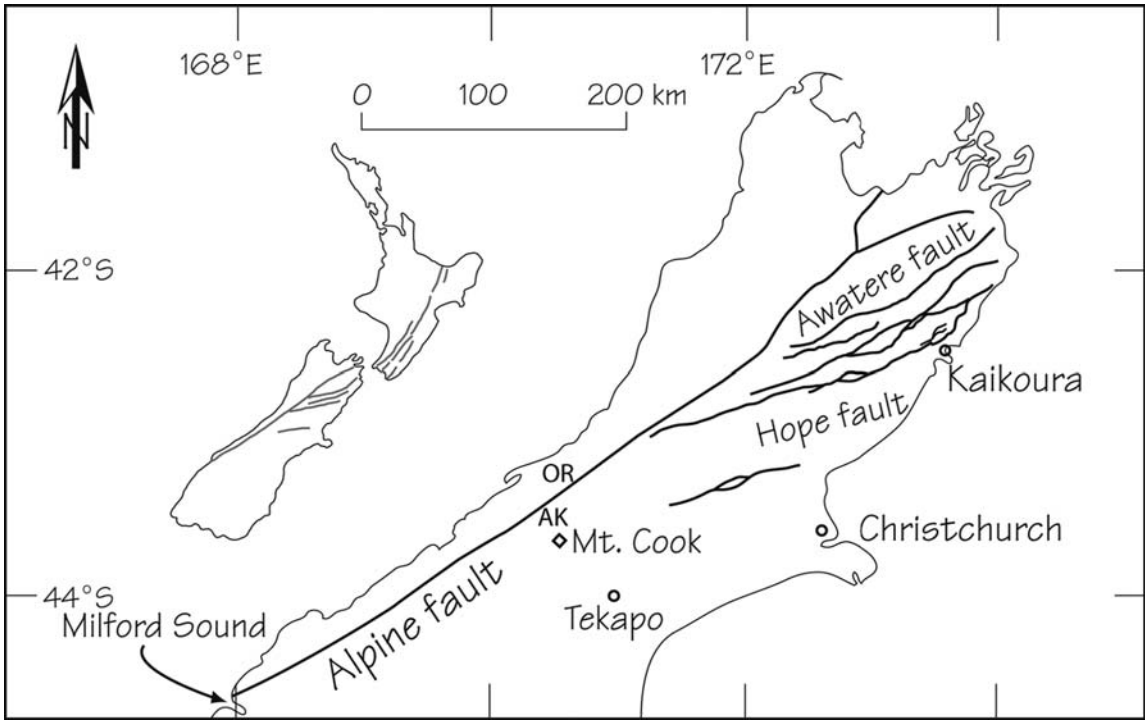

FIGURE 2.1. New Zealand location map. The plate-bounding Alpine fault splits into dextral-oblique thrust faults in the northeast corner of the South Island (the Marlborough district). OR and AK are the Oroko Swamp and Alex Knob tree-ring analysis sites.

FIGURE 2.2. Mt. John scree lichenometry site, east of the Southern Alps of New Zealand. The largest lichen was measured on 546 blocks in the long tongues of talus below rock outcrops of highly fractured, slightly metamorphosed, greywacke sandstone. Buildings at summit are part of an astronomical observatory. Site is at 43° 59′ 19″ S, 170° 28′ 6.67″ E and at an altitude of 815–930 m.

measuring lichens in New Zealand since 1989, so direct comparison of this dataset with those of previous years is not possible unless the data are normalized, in this case to my base year of 1992.

Some Mt. John rockfalls are caused by frequent processes such as frost wedging, but the Figure 2.4 histogram consists of many distinct peaks indicative of pulses of outcrop collapse. These data are meaningful only when compared to my South Island dataset of 37 000 lichen sizes measured at 101 sites. All of the Figure 2.4 prominent lichen-size peaks occur at other sites. Peak B dates to the time of a tree-ring dated Alpine fault earthquake

TABLE 2.1. *Comparison of the precision of lichenometry and tree-ring methods of dating regional seismic shaking events in the South Island of New Zealand*

Dating method	1715 event	1615 event	1580 event
Lichenometry	$n = 10$	$n = 9$	$n = 8$
Mean age, two standard deviations	AD 1716 ± 2.80 years	AD 1613 ± 1.78 years	AD 1579 ± 2.08 years
Tree-ring analyses	$n = 12$	$n = 9$	$n = 9$
Mean age, two standard deviations	AD 1716 ± 2.78 years	AD 1615 ± 2.58 years	AD 1578 ± 3.12 years

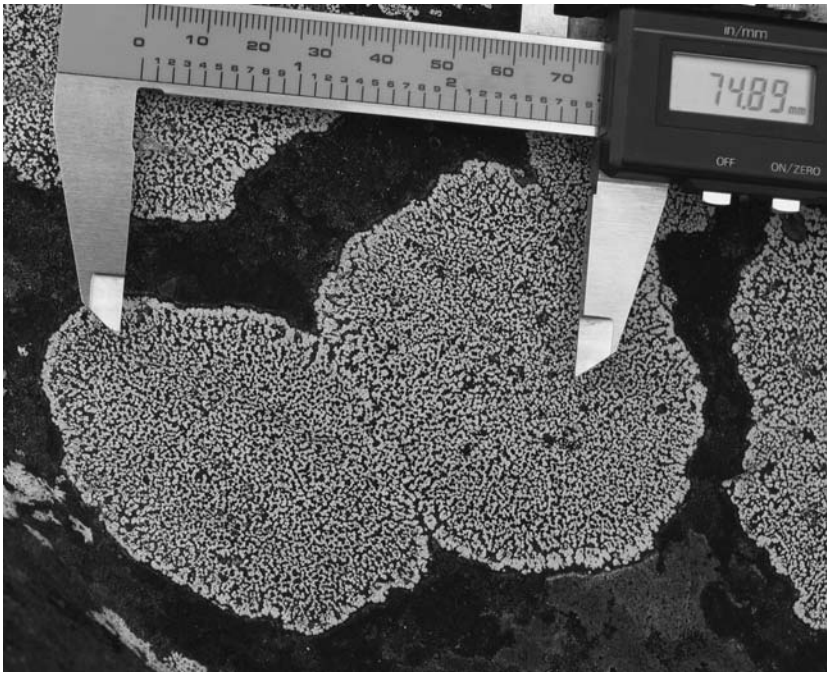

FIGURE 2.3. The longest axes of these two elliptical *Rhizocarpon* subgenus *Rhizocarpon* on this rockfall block both are 74.89 mm, including the black prothallus fungal rim. These date to *c.* AD 1550.

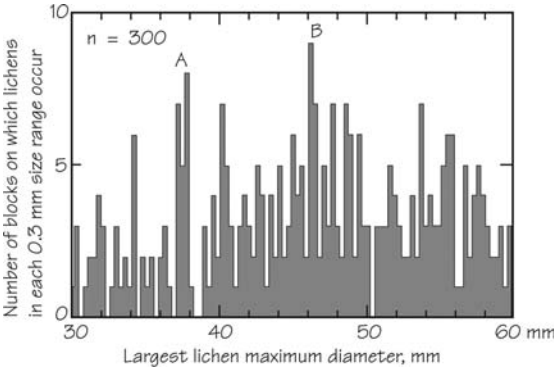

FIGURE 2.4. History of seismic shaking at Mt. John as revealed by histogram of lichen sizes on numerous coseismic rockfalls. Class interval is 0.3 mm. Peak A records two regional seismic shaking events (AD 1788 and 1792 ± 2 years as dated in Figure 6.28 of Bull (2007)). Peak B records the Alpine fault earthquake of AD 1717.

(Table 2.1). Mt. John is 76 km from the Alpine fault. Peak A would be regarded as a single rockfall event if only the Mt. John site is considered. But a twin peak is a defining characteristic for two earthquakes, closely spaced in time, at 67 other sites. Of course some of the smallest peaks are merely dataset noise, but many record weak or distant seismic shaking. A lichen-size peak is indicative of regional seismic shaking if it also occurs at three or more other sites.

Event ages are estimated using the modal value lichen of a lichen-size peak on a standard histogram or by decomposing a composite probability density plot into its component peaks (Bull and Brandon, 1998). Careful selection of the most appropriate class interval or Gaussian kernel size is essential. Unwanted noise is included if too small, and combining of real lichen-size peaks into meaningless peaks results if too large. Comparison of local data with sizes from other sites has led to the realization that using closely

spaced lichen-size peaks is warranted. Fortunately, the rate of lichen growth here is sufficiently fast to separate events only 4–6 years apart, but slow enough to date 1,000-year-old events.

The growth rate of several sections of *Rhizocarpon* subgenus *Rhizocarpon* is the same and was determined at sites of known age (Bull and Brandon, 1998):

$$D = 315.31 - 0.1552t,$$

where D is the mean size of a lichen-size peak and t is the substrate-exposure age in years.

Dating precision and accuracy are excellent. The times of three recent prehistorical Alpine fault earthquakes are summarized in Table 2.1. The tree-ring analyses included both simple counting of annual growth rings and dendrochronologic cross dating. The lichenometry age estimates for these three earthquake events are virtually the same as estimated by tree-ring analyses. Accuracy of lichenometric dating is also ±~2 years in both New Zealand and California (Bull, 2003, 2004, 2007, Figures 6.8 and 6.47). Assuming that age estimates presented here are within ±5 years seems reasonable. This large, precise database allows studies of regional variations in the seismic shaking for a particular earthquake.

2.3 Regional seismic shaking

The size of the 84 mm lichen-size peak varies from site to site, and contouring of these data creates a pattern that is parallel to, and close to, the Alpine fault. The resulting peak-size (seismic-shaking index) map (Figure 2.5) suggests rupture of all of the central section of the Alpine fault at about AD 1490. Tree-ring analyses provide strong support for a major surface rupture at this time. Marked suppressions in annual growth of cedar trees at this time were noted in three Oroko Swamp trees and five Alex Knob trees. The event in these eight trees dates as AD 1487 ± 2.56 years. Decomposition of a lichen probability density plot (Bull, 1996, Figure 14) indicates an age of AD 1488.9 ± 4 years (2σ again). The Figure 2.5 map does not cross the Alpine fault because the climate on the northwest side of the Southern Alps is too wet for *Rhizocarpon* subgenus *Rhizocarpon*. The map would be similar if the Alpine fault were offshore. I next continue this type of analysis for the faults of the Marlborough district.

In Figure 2.6, decomposition of a single Gaussian probability density plot for the times of regional rockfall events at 47 lichenometry sites suggests that three coseismic rockfall events occurred during a 6-year time span in the Marlborough district. Estimated calendric ages for these three regional rockfall events are about AD 1842, 1838,

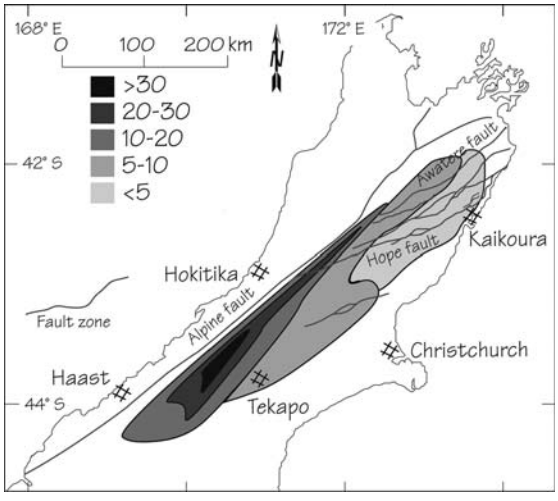

FIGURE 2.5. A seismic-shaking index map for the *c.* AD 1490 Alpine fault earthquake. The peak-size index is the area of a modeled subpopulation relative to the total area of a Gaussian composite probability density plot in the 6 mm range of lichen sizes that bracket the event time.

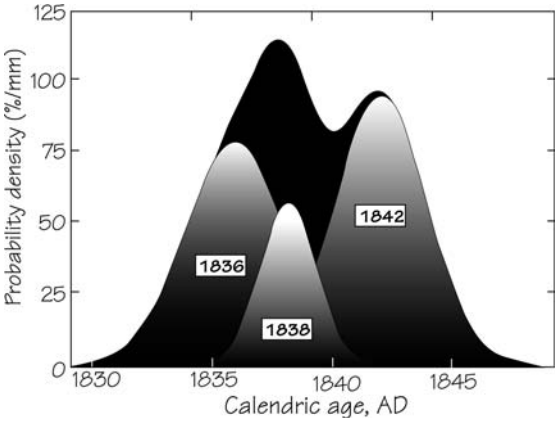

FIGURE 2.6. Decomposition of a Gaussian probability density plot, in black, of the times of regional rockfall events at 47 lichenometry sites. Gaussian kernel size is 1.0 year. (From Figure 22 of Bull and Brandon, 1998.)

and 1836. Can we really separate seismic-shaking events only a few years apart? Seismic-shaking index maps that describe regional patterns of sizes of lichen-size peaks provide an unequivocal answer.

The peak-size pattern for the two older events (Figures 2.6, 2.7A) is suggestive of a composite pattern of seismic shaking resulting from two earthquakes. The smaller event occurred in about AD 1838 near the western edge of the study area. The AD 1836 event occurred along the Conway segment of the Hope fault. The linear area of

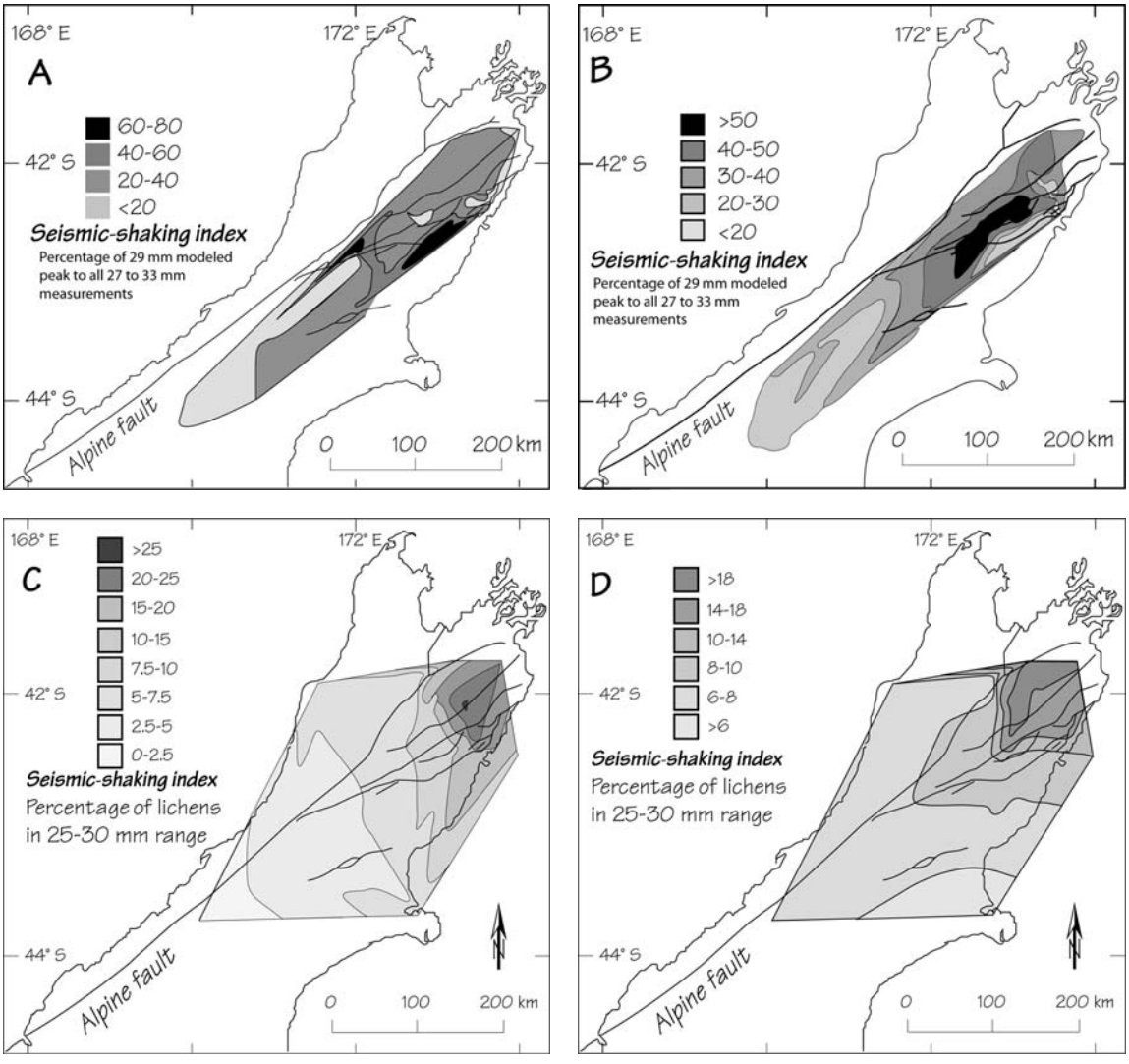

FIGURE 2.7. Seismic-shaking index maps based on regional variations in rockfall abundance. A. Two events at edges of the study region. (From Figure 23A of Bull and Brandon, 1998.) B. Event emanating from center of study region. (Figure 23B of Bull and Brandon, 1998.) C. AD 1848 historical earthquake seismic shaking. (From Figure 6.32C of Bull, 2007.) D. AD 1855 historical earthquake seismic shaking. (From Figure 6.32D of Bull, 2007.)

most intense seismic shaking parallels the fault trace, but continues on to the southwest for another 40 km. This apparent extension of seismic shaking may have resulted as a directivity effect of a fault rupture that had its propagation energy absorbed at the southwest terminus.

The simpler pattern associated with the next oldest seismic-shaking index event (Figure 2.7B) clearly suggests seismic shaking associated with a single large earthquake in about AD 1842 on the Clarence and Elliott faults (between the Hope and Awatere faults on Figure 2.1). The earthquake epicenter, if near the north end, was only about 30 km southwest of the historic AD 1848 surface rupture on the Awatere fault. Peak sizes for the AD ~1842 event are anomalously low near the Conway segment of the Hope fault, most likely because the AD ~1836 earthquake had already dislodged most of the unstable blocks on those hillslopes.

The internal consistency of the two seismic-shaking index maps and the three peaks of Figure 2.6 support the hypothesis of three earthquakes in 6 years. The AD ~1842 Clarence–Elliott earthquake is not included in lists of historical earthquakes (post AD 1840 European settlement) because the first attempt to find a route up the remote Awatere valley was in AD 1850.

The historic Mw magnitude ~7.4 earthquake of 16 October 1848 damaged many cob houses of early settlers. It occurred on the eastern half of the Awatere fault (Grapes *et al*., 1998; Benson *et al*., 2001) A seismic-shaking index map of this event (Figure 2.7C) suggests the same location as the geologic field studies.

A very large Mw magnitude ~8.2 historic earthquake in the southern part of the North Island occurred on 23 January 1855. Beaches were raised as much as 6 m (Hull and McSaveney, 1993) and as much as 12 m of horizontal displacement was noted for the surface rupture (Grapes and Downes, 1997). The intensity of seismic shaking in northeastern Marlborough (Fig. 2.7D) was about the same as the local 1848 event even though the 1855 earthquake epicenter was ~85 km away. Strong seismic shaking extended far to the southwest.

The 1848 and 1855 seismic-shaking index maps both use the percentage of lichens in their respective lichen-size peaks relative to the total number of rockfalls in the 25–30 mm lichen-size range. This allows construction of a map showing the relative seismic shaking for these two events (Figure 2.8). Marlborough lichenometry site responses to seismic shaking range greatly; many new rockfall blocks at some sites, few at others. The southwestern two-thirds of the map clearly shows the progressively greater relative seismic-shaking intensity of the 1855 event. Although the 1848 earthquake was large, comparatively it was quite local. The 1855 earthquake was enormous; it maintained hillslope disruptive power as it rumbled much farther southwest. The hazards potential is much higher for Mw 8 than for Mw 7 earthquakes.

Perhaps these four recent earthquakes in the transpressional plate boundary are related and occurred as a sequence at 6-year intervals. Their temporal spacing and northward spatial progression support this speculation. Figure 2.9 shows the locations of the primary faults, but the secondary cross faults were involved too. Event A was in 1836 on the Conway segment of the Hope fault. Event B was the 1842 earthquake on the Clarence–Elliott faults. Right-lateral displacement of about 7 m (Nicol and Van Dissen, 2002) indicates a Mw magnitude >7.0 earthquake for this event. The magnitude ~7.4 Marlborough earthquake in 1848 (Event C) had a surface rupture whose southwestern end at Barefells Pass (Benson *et al*., 2001) was only 10 km north of the Clarence fault. This 105 km long rupture extends towards the northeast. The M ~ 8.2 Wairarapa earthquake of 1855 (Event D), described by Van Dissen and Berryman (1996), occurred 6 years after the Marlborough earthquake and an additional 85 km farther northeast. Benson *et al*. (2001, p. 1,090) note, "The dextral

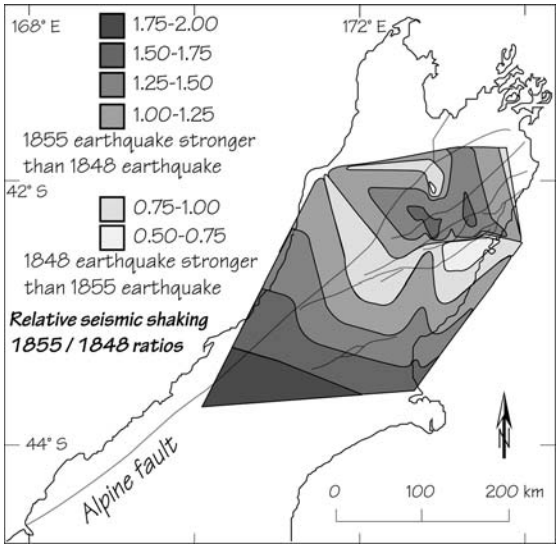

FIGURE 2.8. Relative intensity of seismic shaking (rockfall block abundance) for the Mw magnitude 8.2 Wairarapa earthquake of 1855 (earthquake epicenter in the North Island), compared to the Mw magnitude 7.4 Marlborough earthquake of 1848 (earthquake epicenter on eastern Awatere fault). Either event can be dominant near the Awatere fault, but seismic shaking during 1855 is progressively more important to the southwest. (From Figure 6.33 of Bull, 2007.)

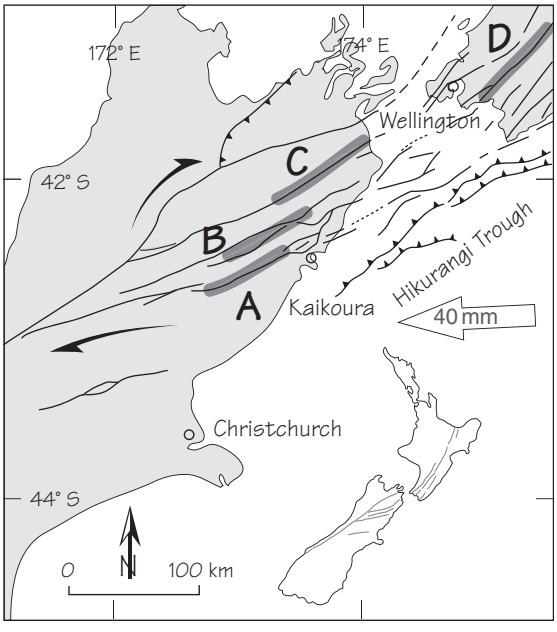

FIGURE 2.9. Sequence of epicentral locations for four large earthquakes in the Marlborough–Wellington plate transpressional zone. (From Figure 6.34 of Bull, 2007.)

strike slip Wairarapa fault can be traced offshore from lower North Island into Cook Strait and to within 20 km of the northeastern end of the Awatere fault (Carter *et al*., 1988). Although there may be no direct fault connection between the two faults, it might be speculated that the 1848 rupture of the Awatere fault precipitated failure of the Wairarapa fault during the 1855 earthquake." This sequence – four earthquakes at 6-year intervals on different fault zones – is unlikely to be repeated. The earthquake-prone mountains near the town of Kaikoura have not experienced hazardous seismic events since this sequence of four earthquakes relieved much of the accumulated stresses on this part of the plate boundary.

2.4 Conclusions

The frequency and intensity of landslide hazards in mountainous landscapes is a function of rock type, climate, and earthquakes. Use of lichens to study geomorphic processes has progressed to where individual rockfall events can be dated with a precision of ±5 years. Spatial variation in abundance of rockfall blocks of a certain age can be used to make seismic-shaking intensity maps as good as Mercalli intensity maps. These maps identify the most likely fault(s) for a given time of earthquake(s), and the approximate position of the earthquake epicenter. Series of maps may depict earthquake sequences as stress is transferred from fault to fault.

References

Benson, A. M., Little, T. A., Van Dissen, R. J., Hill, N. and Townsend, D. B. (2001). Late Quaternary paleoseismic history and surface rupture characteristics of the eastern Awatere strike-slip fault, New Zealand. *Geological Society of America Bulletin*, **113**, 1079–1091.

Bull, W. B. (1996). Prehistorical earthquakes on the Alpine fault, New Zealand. *Journal of Geophysical Research, Solid Earth, Special Section "Paleoseismology"*, **101**, 6037–6050.

Bull, W. B. (2003). Lichenometry dating of coseismic changes to a New Zealand landslide complex. *Annals of Geophysics*, **46**, 1155–1167.

Bull, W. B. (2004). Sierra Nevada earthquake history from lichens on rockfall blocks. Sierra Nature Notes, http://www.yosemite.org/naturenotes/LichenIntro.htm.

Bull, W. B. (2007). *Tectonic Geomorphology of Mountains: A New Approach to Paleoseismology*. Oxford: Blackwell Publishing.

Bull, W. B. and Brandon, M. T. (1998). Lichen dating of earthquake-generated regional rockfall events, Southern Alps, New Zealand. *Geological Society of America Bulletin*, **110**, 60–84.

Carter, L., Lewis, K. B. and Davey, F. (1988). Faults in Cook Strait and their bearing on the structure of central New Zealand. *New Zealand Journal of Geology and Geophysics*, **31**, 431–446.

Grapes, R. and Downes, G. (1997). The 1855 Wairarapa, New Zealand, earthquake-analysis of historical data. *Royal Society of New Zealand Bulletin*, **30**, 271–368.

Grapes, R., Little, T. A. and Downes G. (1998). Rupturing of the Awatere Fault during the 1848 October 16 Marlborough earthquake, New Zealand: historical and present day evidence. *New Zealand Journal of Geology and Geophysics*, **41**, 387–399.

Hull A. G. and McSaveney M. J. (1993). *A 7000-year Record of Great Earthquakes at Turakirae Head, Wellington, New Zealand*. New Zealand Earthquake Commission Research Paper 011, Project 93/139.

Nicol, A. and Van Dissen, R. (2002). Up-dip partitioning of displacement components on the oblique-slip Clarence Fault, New Zealand. *Journal of Structural Geology*, **24**, 1521–1535.

Van Dissen, R. J. and Berryman, K. R. (1996). Surface rupture earthquakes over the last 100 years in the Wellington region, New Zealand, and implications for ground shaking hazard. *Journal of Geophysical Research*, **101**, 5999–6019.